Materials Today Bio 19 (2023) 100549

Contents lists available at ScienceDirect

Materials Today Bio

journal homepage: www.journals.elsevier.com/materials-today-bio

Engineering exosomes by three-dimensional porous scaffold culture of human umbilical cord mesenchymal stem cells promote osteochondral repair

Zineng Yan [a,b,1], Han Yin [b,1], Jiang Wu [a,b,1], Guangzhao Tian [b,c], Muzhe Li [b], Zhiyao Liao [b,c], Songlin He [b,c], Haoyuan Deng [b,c], Chao Ning [b], Zhengang Ding [a,b], Xun Yuan [a,b], Xiang Sui [b], Mingxue Chen [d,***], Shuyun Liu [b,**], Quanyi Guo [b,*]

[a] Guizhou Medical University, Guiyang, 550004, Guizhou, China
[b] Institute of Orthopedics, Chinese PLA General Hospital; Beijing Key Laboratory of Regenerative Medicine in Orthopedics; Key Laboratory of Musculoskeletal Trauma & War Injuries PLA; No. 28 Fuxing Road, Haidian District, Beijing, 100853, China
[c] School of Medicine, Nankai University, Tianjin, 300071, China
[d] Department of Orthopaedic Surgery, Beijing Jishuitan Hospital, Peking University Fourth School of Clinical Medicine, No. 31 Xinjiekou East Street, Xicheng District, Beijing, 100035, China

ARTICLE INFO

Keywords:
Three-dimensional scaffold culture
Exosomes
Cartilage repair
miRNA

ABSTRACT

Improving the poor microenvironment in the joint cavity has potential for treating cartilage injury, and mesenchymal stem cell (MSC)-derived exosomes (MSC-Exos), which can modulate cellular behavior, are becoming a new cell-free therapy for cartilage repair. Here, we used acellular cartilage extracellular matrix (ACECM) to prepare 3D scaffolds and 2D substrates by low-temperature deposition modeling (LDM) and tape casting. We aimed to investigate whether MSC-Exos cultured on scaffolds of different dimensions could improve the poor joint cavity microenvironment caused by cartilage injury and to explore the related mechanisms. In vitro experiments showed that exosomes derived from MSCs cultured on three-dimensional (3D) scaffolds (3D-Exos) had increased efficiency. In short-term animal experiments, compared with exosomes derived from MSCs cultured in a two-dimensional (2D) environment (2D-Exos), 3D-Exos had a stronger ability to regulate the joint cavity microenvironment. Long-term animal studies confirmed the therapeutic efficacy of 3D-Exos over 2D-Exos. Thus, 3D-Exos were applied in the rat knee osteochondral defect model after adsorption in the micropores of the scaffold and combined with subsequent articular cavity injections, and they showed a stronger cartilage repair ability. These findings provide a new strategy for repairing articular cartilage damage. Furthermore, miRNA sequencing indicated that the function of 3D-Exos may be associated with high expression of miRNAs. Thus, our study provides valuable insights for the design of 3D-Exos to promote cartilage regeneration.

1. Introduction

Articular cartilage lacks vascular, nerve and lymphatic tissue, making it repair difficult after damage. Current treatment methods can regenerate only fibrocartilage with poor structure and function. The realization on of safe and sustainable cartilage repair is of great significance for reducing the societal burden of articular cartilage damage. Previous studies have shown that the inflammatory microenvironment generated by articular cartilage injury is significance for chondrocyte hypertrophy, extracellular matrix degradation, bone formation and the development of osteoarthritis [1]. Synovial inflammation is associated with knee edema and dysfunction, and plays a role in the occurrence and development of osteoarthritis [2]. In addition, immune cells represented by M2 macrophages can not only suppress inflammation, but also regulate the repair of damaged tissues [3]. The key to repairing articular cartilage damage is improving the regenerative microenvironment of the joint cavity,

* Corresponding author.
** Corresponding author.
*** Corresponding author.
E-mail addresses: yanzineng16@163.com (Z. Yan), chenmingxueplagh@hotmail.com (M. Chen), clear_ann@163.com (S. Liu), doctorguo_301@163.com (Q. Guo).
[1] Three authors contributed equally to this work.

https://doi.org/10.1016/j.mtbio.2023.100549
Received 14 November 2022; Received in revised form 31 December 2022; Accepted 11 January 2023
Available online 20 January 2023
2590-0064/© 2023 The Authors. Published by Elsevier Ltd. This is an open access article under the CC BY-NC-ND license (http://creativecommons.org/licenses/by-nc-nd/4.0/).

including enhancing the recruitment of endogenous stem cells, local immune regulation, and the protection of chondrocytes and their matrix. Exosomes are paracrine products of MSCs, and various nucleic acids, proteins and other molecules encapsulated in their lipid molecular membranes can promote cell-to-cell communication and thus play a major role in mediating tissue repair and regeneration. Most of the exosomes obtained in previous studies were based on monolayer 2D cultures; however, the native microenvironment and MSCs of 2D cultures are very different, and their stemness (phenotype) and function (proliferation, differentiation and immune regulation) are therefore greatly restricted [4], which also limits the therapeutic efficacy of exosomes. In recent years, numerous studies have shown that the use of 3D scaffolds, microcarriers and cell aggregates can maintain the expression of MSC surface markers and promote their proliferation and immune paracrine functions. Exosomes encapsulate various nucleic acids, proteins and other signaling molecules, so they are regarded as important carriers for intercellular signaling [5], and their encapsulation is affected by the microenvironment in which they are located. A study evaluated the effect of Cellhesion VP (a water-insoluble material composed of chitin-based polysaccharide fibers); the results showed that 3D-EVs exhibited different proteins than extracellular vesicle-derived human umbilical cord mesenchymal stem cells cultured in a 2D environment (2D-EVs), and their therapeutic properties are also distinct from those of 2D-EVs [6]. A study compared the microRNAs and proteins of EVs secreted by tumor cells in three-dimensional and two-dimensional culture environments, and the results showed that microRNAs were upregulated overall in three-dimensional conditions, while proteins were downregulated [7]. 3D culture systems can be either scaffold-based, with natural or artificial solid scaffolds, or scaffold-free, such as spheroids. 3D spheroids enhanced cell–cell interactions and therefore had an advantage over normal 2D culture, but spheroids could not simulate the cell-matrix interaction, which is ubiquitous in the body [8]. Scaffold biophysical cues can provide MSCs with a perceptible microenvironment and stimulate ideal cell behavior through cell-matrix interactions. An increasing number of studies have shown that cells can respond to changes in the microenvironment through morphological changes and then regulate their paracrine function through mechanical transduction of corresponding signals, and their secreted exosomes may also change.

Derived from natural cartilage tissue ACECM(acellular extracellular matrix)is theoretically more suitable for cartilage repair than other natural or synthetic materials in structure and composition. Previous studies by our team showed that WPU scaffolds combined with ACECM successfully induced chondrogenic differentiation of MSC in vitro [9]. In situ implantation of acellular ACECM scaffold could effectively promote the repair and regeneration of articular cartilage defects [10].3D printing technology is widely used in the field of tissue engineering, and its manufacturing mode can be used to build a 3D culture microenvironment with more optimized structure. In addition, the 3D-printed sponge scaffolds prepared by low-temperature deposition modeling (LDM) and freeze drying have high porosity and pore connectivity, and the interconnected micropores of the scaffolds enhance the surface roughness of the scaffolds, which greatly promotes cell–cell and cell-scaffold interactions. At present, it is known that the topology of scaffolds can enhance the paracrine function of MSCs [11], but there are few studies on the regulation of the joint cavity microenvironment by exosomes secreted by MSCs cultured in porous scaffolds. In this study, human umbilical cord mesenchymal stem cells (hUMSCs) were cultured on 3D printed acellular cartilage extracellular matrix (ACECM) scaffolds and 2D ACECM film, and the exosomes in the culture supernatant were obtained and characterized. We explored the biological effects of exosomes in different culture environments on bone marrow mesenchymal stem cells (BMSCs) in vitro, including the effects on proliferation, migration and chondrogenic differentiation in the cartilage regeneration microenvironment. In addition, we inestigated the differences in immune regulation of exosomes from different culture sources. Moreover, we initially explored the differences in miRNAs between 3D-Exos and 2D-Exos by miRNA sequencing and performed GO/KEGG analysis. Finally, we applied exosomes in a rat knee osteochondral defect model to study the enhancement of in situ cartilage repair mediated by 3D-Exos. An overview of the study design is shown in Fig. 1.

2. Materials and methods

2.1. hUMSC culture

The isolation and culture of hUMSCs were carried out according to a previous study [10]. Generally, Wharton's jelly was obtained from an umbilical cord. The tissue was cut into 1 mm^3 pieces and spread on gauze. The gauze was placed in a culture flask. The medium was changed every 2–3 days. Detailed experimental procedures are available in Supplementary Information Section 1.1.

2.2. Synthesis and characterization of 3D ECM scaffolds and 2D ECM film

The preparation of porcine cartilage extracellular matrix was based on previous research results. The acellular cartilage matrix was washed with PBS and then made up as a 5% w/v suspension. The acellular cartilage matrix was used to prepare 3D scaffolds and 2D substrates by low temperature deposition modeling (LDM) and tape casting. The samples before and after cell seeding were characterized by scanning electron microscopy (SEM) and confocal microscopy. Detailed experimental procedures are available in Supplementary Information Sections 1.2.

2.3. Exo extraction and characteristics

Before extracting exosomes (Exos), the medium was replaced with serum medium without exosomes for 48 h, the supernatant was collected, and the exosomes were separated by differ-ential ultracentrifugation. Exosomal target proteins CD9, CD63, Calnexin and TSG101 were detected by western blot. Exos images were acquired using a transmission electron microscope (TEM). The particle size distribu-tion and concentration of Exos were determined with NTA. Detailed experimental procedures are available in Supplementary Information Sections 1.3.

2.4. Labeling and uptake of exos

Exos were labeled with the red fluorescent dye PKH26. To visualize the internalization of Exos, identically labeled Exos were incubated with MSCs or macrophages for 12 h at 37 °C. Cells were fixed in 4% paraformaldehyde for 30 min at room temperature, and nuclei were stained with DAPI. All samples were imaged under a confocal microscope. Detailed experimental procedures are available in Supplementary Information Section 1.3.2.

2.5. Effect of exos on BMSCs, chondrocytes, and macrophages in vitro

2.5.1. Effects of exos on the viability of BMSCs

To evaluate the effect of different Exos on cell proliferation, EdU, Cell cycle detection and Cell Counting Kit-8 (CCK-8) assays were used. Detailed experimental procedures are available in Supplementary Information Section 1.4.

2.5.2. Effects of exos on the migration of BMSCs

To evaluate the migration of BMSCs after different Exo treatments, a scratch healing assay and a Transwell chamber assay were employed. Detailed experimental procedures are available in Supplementary Information Section 1.5.

2.5.3. Ability of exos to promote chondrogenic differentiation in vitro

BMSCs seeded in plates were used to evaluate the short-term effect of different Exos on the chondrogenic differentiation potential of BMSCs (7

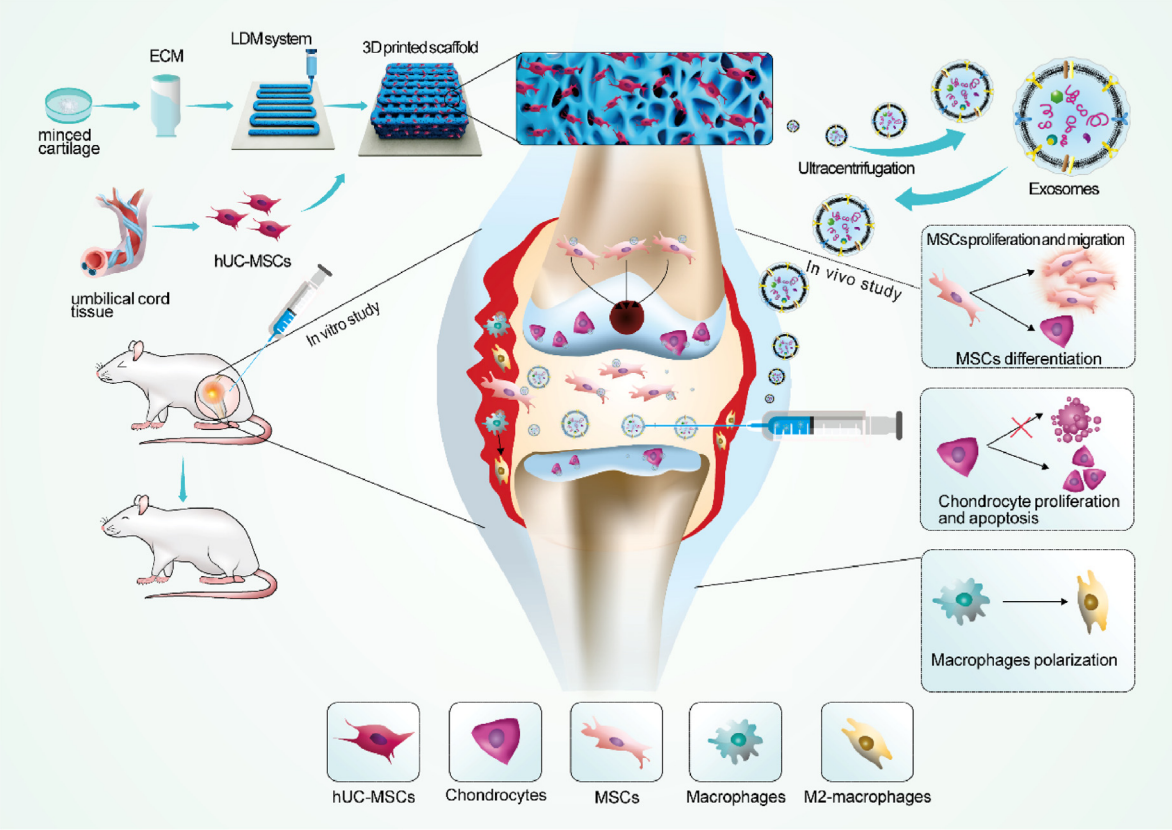

Fig. 1. Schematic diagram of the overall study design.

days). The MSC pellets were used to clarify the long-term effect of different Exos on the chondrogenic differentiation potential of BMSCs (14 days). After 7 and 14 days of coculture in three different media, the level of chondrogenesis was evaluated via Alcian blue staining. Finally, the expression of chondrogenesis-related genes at 7 days was detected by RT–qPCR and immunofluorescence. The relevant primer sequences are shown in Table S1. Detailed experimental procedures are available in Supplementary Information Section 1.6.

2.5.4. Effects of exos on macrophages polarization

RT-qPCR and immunofluorescence techniques were used to compare the effects of different foreign substances on the polarization ability of macrophages (BMDMs and Raw264.7). For RT-qPCR, the experimental group used the medium containing different Exos (25 μg/mL), and the control group used the medium containing the same amount of PBS. Macrophages were seeded into 6-well plates, with 3 wells in each group, and cultured in the above three media for 24 h. The RT-qPCR method was reported in our team's previous study [3]. ***CD206, Arg-1*** **and** ***CD163*** were used as target genes. The relevant primer sequences are shown in Table S1. The LightCycler 480 system was used to quantify gene expression. The primary antibodies used for immunofluorescence staining were anti-CD206 (M2 marker). All experiments were performed on three independent replicates. Detailed experimental procedures are available in Supplementary Information Section 1.7.

2.5.5. Effects of exos on chondrocytes

V-FITC/PI and CCK-8 were used to evaluate the effects of different external matrices on chondrocyte viability and apoptosis. Briefly, chondrocytes were co-cultrued with three different medium (exo-free, 2D-Exo, 3D-Exo), followed by 10 ng/mL IL-1β challenge for 24 h.The apoptosis inhibition of chondrocytes was detected by flow cytometry. Detailed experimental procedures are available in Supplementary Information Sections 1.8.

2.5.6. NLRP3 inflammasome activation of macrophages

Raw246.7 were seeded in 24-well plates and cocultured with different Exos (25μg/ml) for 48 h. After 4 h of cocultre with LPS (100 ng/mL, Sigma), NLRP3 inflammasome activation was induced by challenging cells with nigericin (10 mM, MCE) for 30 min Raw246.7 in 24-well plates were used for immunofluorescence staining to detect the expression of NLRP3-associated signaling proteins. (Anti- NLRP3 antibody, BIOSS,1:100; *Anti*–NF–kB p65 antibody, BIOSS, 1:100).

2.6. In vivo animal experiment

2.6.1. Biodistribution of exos

To assess the effects of different delivery methods on the exosome biodistribution, 3D-Exos were stained with the fluorescent dye DiO, and then the scaffold loaded with DiO-labeled Exos was implanted into the osteochondral defect model, while joint cavity injection of DiO-labeled 3D-Exos was performed for the control group. Detailed experimental procedures are available in Supplementary Information Section 2.1.1.

Exosomes were stained with DiD (C1039, Beyotime) according to the manufacture's protocals. Fluorescently labeled exosomes were implanted into the knee joint of rats (the in-jection group and the exosomes-loaded group) . Living imaging was performed on an IVIS (PerkinElmer) at 1day, 3day and 5day. Fluorescence signaling was analyzed using Living-Image soft-ware.

2.6.2. Exos loading

3D-Exos (25 μg/mL) were loaded on a hierarchical macro-microporous scaffold at a saturated adsorption volume under sterile conditions, and the scaffold was placed at 4 °C for 5 h for full adsorption of Exos into the surface micropores. Exos in surface micropores were observed by SEM.

2.6.3. Regulatory effect of exos on the articular cavity microenvironment

Nine 6-week-old male Sprague–Dawley rats (250 ± 50 g) were randomly allocated to three groups, with 3 rats in each group: the control group, the 2D-Exo group and the 3D-Exo group. For all groups, an osteochondral defect (2.0 mm in diameter and 1 mm in depth) was created by drilling with a trephine. After surgery, the rats in the control group were injected with 50 μL of PBS. For the 2D-Exo group and 3D-Exo group, the knee joint cavity was injected with an equal volume of 25 μg/mL Exos, and the injections were repeated every 5 days. The rats in each group were sacrificed after 14 days, and the distal femur and joint synovium were collected. The levels of immunoregulation and migration of endogenous MSCs were assessed by immunofluorescence staining. Detailed experimental procedures are available in Supplementary Information Section 2.1.2.

2.6.4. In vivo immune response evaluation

The exosomes and scaffolds were implanted subcutaneously into the back skin of SD rats to evaluate their biocompatibility in vivo. At 1 week after implantation, rats were sacrificed, and H&E staining was performed to evaluate histological changes.

2.6.5. Reparative effect of exos on osteochondral defects

Thirty 6-week-old male Sprague–Dawley rats (250 ± 50 g) were randomly allocated to five groups: (A) the control group, (B) the 2D-Exo group, (C) the 3D-Exo group, (D) the scaffold group, and (E) the 3D-Exo-loaded scaffold group (n = 6 for each group). Details of the surgery procedure in the S.2.1.2. The animals in the control group and scaffold groups were injected with 50 μL of PBS in the knee joint cavity. The animals in the Exo- and 3D-Exo-loaded groups were injected with an equal volume of 2D-Exo or 3D-Exo suspension at a concentration of 25 μg/mL. Subsequently, injections were administered once every 5 days for a total of 3 injections. The International Cartilage Repair Society (ICRS) macroscopic evaluation criteria for cartilage repair (**Table S2**) and microcomputed tomography (micro-CT) analysis were used to preliminarily analyze the cartilage repair effect and the regeneration of subchondral bone in the defect area. For histological examination, hematoxylin and eosin (H&E) was used to evaluate tissue morphology, and safranin O/fast green and Sirius red staining were used to evaluate the arrangement and distribution of collagen. Immunohistochemical staining of type II collagen (COL II) was used to detect the COL II content. The staining results of the above sections were blindly scored by three researchers in related fields according to a histomorphometric scoring system to evaluate the effect of each treatment on the repair of cartilage and subchondral bone (**Table S3**). Detailed experimental procedures are available in Supplementary Information Section 2.1.3.

2.7. Exo miRNA sequencing and data analysis

Total RNA was isolated using the mirVana miRNA Isolation Kit (Ambion) according to the manufacturer's instructions. Total RNA was quantified using a Nanodrop 2000 (Thermo Fisher Scientific Inc., USA). Total RNA was evaluated using an Agilent 2100 Bioanalyzer (Agilent Technology, USA) to assess the integrity of RNA. One microgram of total RNA from each sample was used to construct small RNA libraries using the NEBNext Small RNA Library Prep Set for Illumina kit (Cat. No. NEB#E7330S, NEB, USA) according to the manufacturer's protocol. Differentially expressed miRNAs were calculated and filtered with a q value < 0.05 and FC > 2 or FC < 0.5 as thresholds. Experiments with biological replicates were analyzed using the DEG algorithm in the R package for q-values, and Audic Claverie statistics was used for experiments without biological replicates. GO enrichment and KEGG pathway enrichment analyses of differentially expressed miRNA–target genes were performed in R language based on hypergeometric distribution.

2.8. Statistical analysis

All data are shown as the mean ± standard deviation (SD). One-way ANOVA or Student's *t*-test was used to evaluate differences among groups using SPSS 17.0 statistical software. *$p < 0.05$ represents the threshold for statistical significance.

3. Results

3.1. Characterization of 2D ECM films and 3D-printed scaffolds

The microstructures of the 2D ECM films and 3D-printed scaffolds were characterized by SEM. The SEM results under different magnifications are shown in Fig. 2a and 2c. Fig. 2a shows that a layered and uniform large microporous structure formed in the 3D-printed scaffolds, and many highly interconnected microporous structures could be observed on the printed fiber surface. However, the 2D ECM film was relatively smooth and had some folds, but there was no obvious porous structure (Fig. 2c). These two different microstructures could affect the cellular behavior and function of hUMSCs on the surface.

The morphology and adhesion behavior of hUMSCs on the surface of cultured carriers in different dimensions were observed by SEM and cytoskelet fluoresce staining. The results showed that hUMSCs could adhere to the surface of both the 2D ECM film and the 3D-printed scaffold and spread well (Fig. 2b,2d,2e and 2g). However, compared to the hUMSCs on 2D ECM film, the hUMSCs on the 3D-printed scaffolds exhibited a more characteristic spindle-shaped morphology and more prominent cell clusters.

Cellular live/dead staining was used to assess cell viability. After 7 days of culture, hUMSCs were able to grow on both 2D ECM films and 3D-printed scaffolds. Confocal microscopy results showed that both carriers could maintain hUMSCs in a viable state (green), and almost no dead cells (red) were observed (Fig. 2f and 2h). The results showed that both carriers had good cytocompatibility. Compared with hUMSCs on 2D ECM films, hUMSCs on the 3D-printed scaffolds grew uniformly along the printed fibers (Fig. 2f). The three-dimensional scaffolds provide hUMSCs with a larger growth space, and their three-dimensional porous structure also enables a higher local cell density, which makes it easier for the cells to form cell aggregates and thus provides more opportunities for cells to come into contact and interact with surrounding cells.

3.2. Identification of exos

TEM results showed that 3D-Exos and 2D-Exos exhibited a typical bilayer biofilm structure with particle sizes ranging from 30 to 150 nm (Fig. 2i). The NTA results showed that the average particle size distribution of 3D-Exos was 69 nm (Fig. 2i), and the average particle size distribution of 2D-Exos was 131 nm (Fig. 2i). The NTA results showed that the particle size of 3D-Exos was significantly smaller than that of 2D-Exos. WB detection results showed that both 3D-Exos and 2D-Exos highly expressed the exosome marker proteins CD9, CD63, and TSG101 but not CANX (Fig. 2j).

3.3. Uptake of exos

The internalization of Exos by the targeted cells is necessary for their biological functions, so we investigated whether macrophages and BMSCs could phagocytose 2D-Exos and 3D-Exos in vitro. PKH26-labeled 2D-Exos (red) and PKH26-labeled 3D-Exos (red) were cocultured with macrophages and BMSCs for 24 h, after which they were placed under a confocal microscope for observation. As shown in Fig. 2k, a strong enrichment of the red fluorescence signal was observed in both

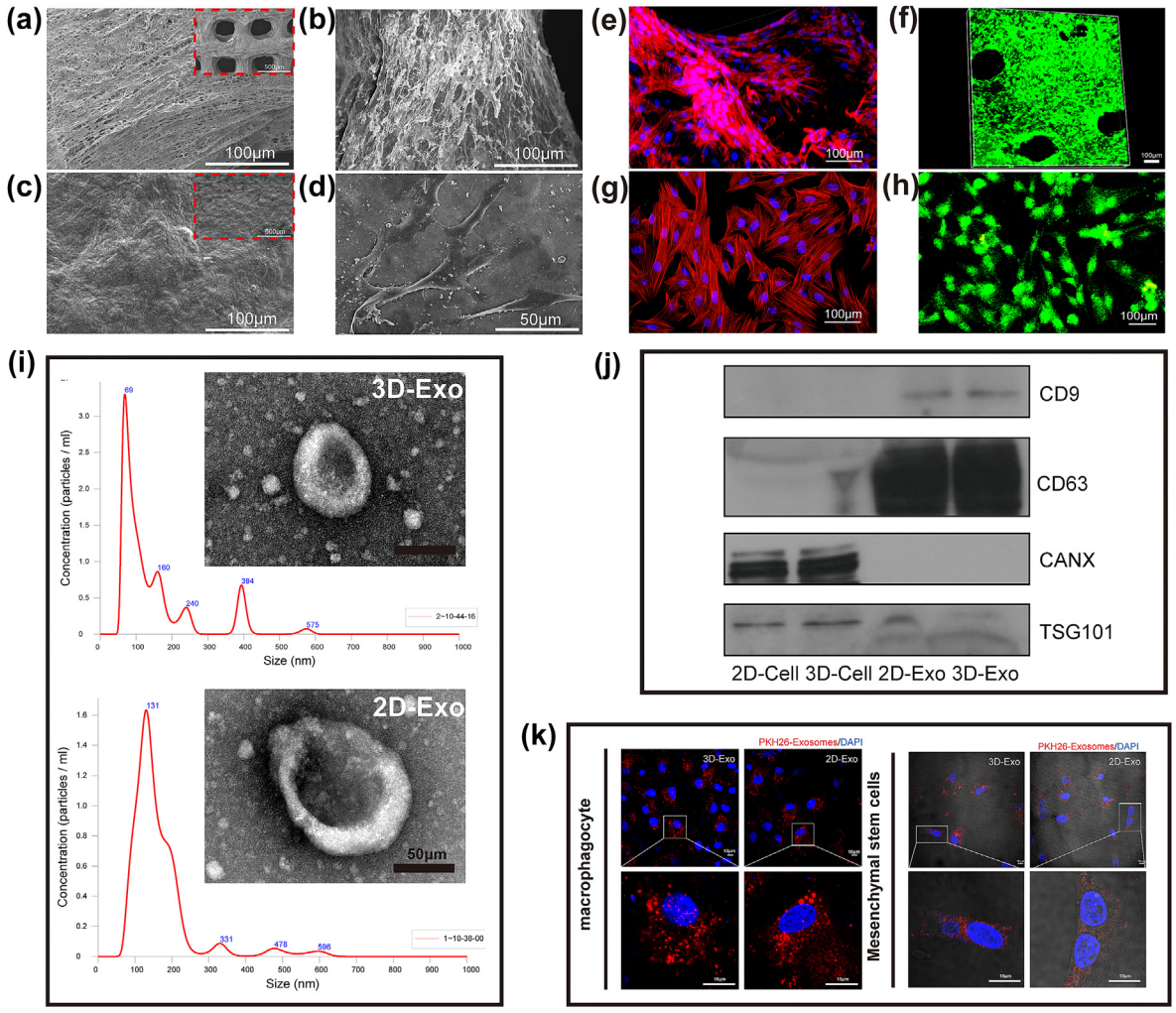

Fig. 2. Characterization of ECM materials and cell growth. (a, c) SEM micrographs of the 3D-printed scaffold and 2D ECM film. (b, d) SEM micrographs of cell adhesion on the 3D ECM scaffold and 2D ECM film. (e, g) F-actin immunofluorescence of cells grown on the 3D ECM scaffold and 2D ECM film. (f, h) Images of cell growth on the 3D ECM scaffold and 2D ECM film by CAM/PI staining. (i) Representative TEM images and NTA analysis of 3D-Exos and 2D-Exos. Scale bar = 50 μm. (j) Western blot analysis of protein markers of Exos and cells in 3D or 2D culture. (k) Uptake of 3D-Exos by macrophages and BMSCs detected by confocal microscopy.

macrophages and BMSCs, and both 2D-Exos and 3D-Exos were internalized by macrophages and BMSCs.

3.4. *Effect of exos on the proliferation and migration of BMSCs*

The results of CCK-8 assays clearly showed that on the first day, compared with the control treatment, 2D-Exos and 3D-Exos did not promote the proliferation of BMSCs. However, both 2D-Exos and 3D-Exos significantly promoted the proliferation of BMSCs at 3 and 7 days. The ability of 3D-Exos to promote the proliferation of BMSCs was significantly better than that of 2D-Exos, and there was a significant difference between the two (Fig. 3c). EdU fluorescence staining was used to detect the effects of 2D-Exos and 3D-Exos on the proliferation of BMSCs. As shown in Fig. 3a, both 2D-Exos and 3D-Exos promoted the proliferation of BMSCs. However, 3D-Exos had a stronger effect. Analysis of the proportion of EdU-stained cells (orange) showed that there were significantly more positive cells in the 3D-exo group than in the 2D-exo group or the control group, and the difference was significant (Fig. 3b).

Therefore, we next selected different Exos (2D-Exos and 3D-Exos) to treat BMSCs and analyzed their effects on the BMSC cycle after 24 h of treatment using flow cytometry. According to the cell cycle results, we concluded that the proportion of BMSCs in S phase, which was important for DNA replication after 3D-Exo treatment, was significantly greater than that observed for the 2D-Exo-treated cells and the control cells, while the proportion of cells in G1 phase was decreased (Fig. 3d). Finally, we demonstrated that 3D-Exos could promote BMSC proliferation by modulating the cell cycle. The above results indicated that 3D-Exos were better able to promote the proliferation of BMSCs than 2D-Exos.

Scratch experiments and Transwell experiments were used to analyze the effects of 2D-Exos and 3D-Exos on the migration of BMSCs in vitro. As shown in Fig. 4a, the cells treated with 2D-Exos and 3D-Exos covered the scratched area earlier than the control cells. However, the effect of 3D-Exo treatment was more obvious than that of 2D-Exo treatment, indicating that 3D-Exos were more efficient than 2D-Exos in promoting BMSC migration in vitro. Statistical analysis of the scratch width also confirmed that the 3D-exo group had the best scratch healing (Fig. 4b). Then, we used Transwell experiments to analyze the effects of 3D-Exos and 2D-Exos on the vertical migration of BMSCs. Crystal violet staining images showed that more migrated BMSCs were observed in the 2D-Exo group and 3D-Exo group at 12 h and 24 h than in the control group. However, the 3D-Exo group exhibited the most migrated cells (Fig. 4c). Statistical analysis of the number of cells showed that the migration effect of the 3D-exo group was the strongest at different time points (Fig. 4d).

We also confirmed that 3D-Exos can promote the migration of BMSCs in vivo. Immunofluorescence staining of regenerated articular cartilage tissue specimens from the three groups was performed after 14 days of

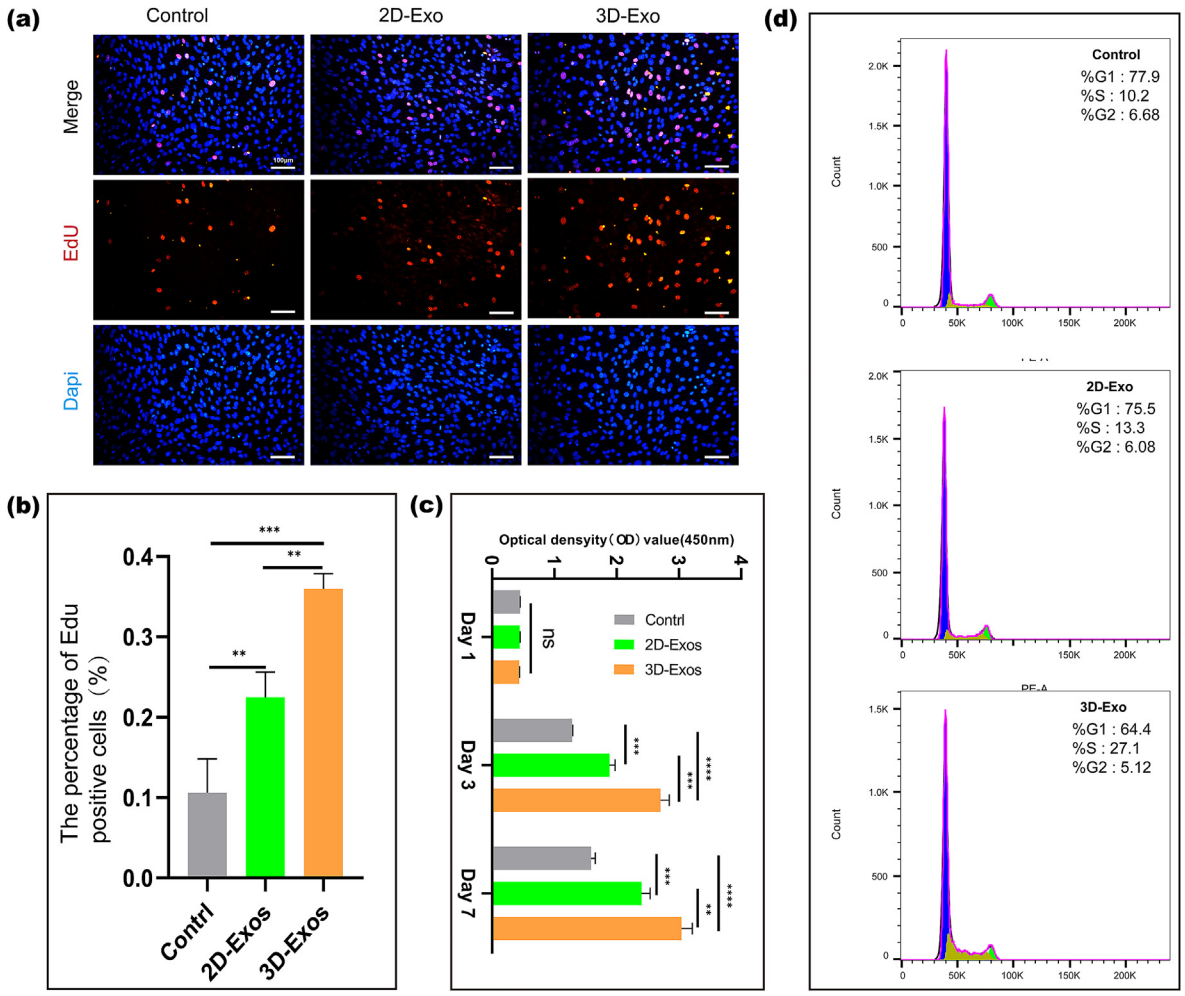

Fig. 3. Effects of different Exos on the proliferation of BMSCs. (a) Immunofluorescence micrographs obtained after EdU staining (EdU: orange, nucleus: blue). Scale bar = 10 μm. (b) Statistical plot of the percentage of EdU-positive cells. (n = 3) (c) CCK-8 results of BMSC proliferation under treatment with 2D-Exos and 3D-Exos. Data are presented as the mean ± SD (n = 3). (d) Flow cytometry results of the cell cycle of BMSCs treated with different Exos for 24 h (**P < 0.01, ***P < 0.005, ****P < 0.001; ns means no significant difference). **(n = 3).**" should be replaced with "(d) Flow cytometry results of the cell cycle of BMSCs treated with different Exos for 24 h (**P < 0.01, ***P < 0.005, ****P < 0.001; ns means no significant difference).

repair in the animal model. The immunofluorescence results showed that the number of CD73 and CD105 double-positive cells in the regenerated tissue was significantly higher in the 3D-exo and 2D-exo groups than in the control group (Fig. 4e); however, the 3D-exo group had the most CD73 and CD105 double-positive cells among the three groups. The statistical results also showed the most CD73 and CD105 double-positive cells in the 3D-exo group (Fig. 4f). These results indicated that compared to 2D-Exos, 3D-Exos significantly increased the migration of endogenous BMSCs to the defect area and promoted articular cartilage regeneration.

3.5. *Effect of exos on chondrogenic differentiation of BMSCs in vitro*

To explore whether 2D-Exos and 3D-Exos are capable of promoting chondrogenic differentiation of BMSCs, we treated BMSCs with 2D-Exos and 3D-Exos for 7 days. The results of COL II staining (Fig. 5a) and Alcian blue staining (Fig. 5b) showed that the 2D-Exo group and the 3D-Exo group had a more chondrogenic phenotype than the control group, but the 3D-Exo group had the strongest chondrogenic phenotype. The chondrogenic phenotype was strongest in the 3D-Exo group among the three groups, and the chondrogenic differentiation of BMSCs was promoted the most strongly in this group. In our experiment, we used a cell pellet culture method to induce chondrogenic differentiation of BMSCs in vitro, according to previous studies. After BMSCs were induced in chondrogenic differentiation medium with 2D-Exos (25 μg/mL) or 3D-Exos (25 μg/mL) for 14 days, we carried out histological staining to qualitatively evaluate chondrogenesis in the cell pellets. As shown in Fig. 5c, Alcian blue staining showed that the 2D-Exo group and the 3D-Exo group had a more chondrogenic phenotype than the control group, but the 3D-Exo group had a stronger chondrogenic phenotype. The chondrogenic phenotype in the 3D-Exo group was strongest among the three groups, and the chondrogenic differentiation of BMSCs was promoted the most strongly in this group. Finally, the expression of the *ACAN, COL II*, and *Sox9* genes in different groups was further studied, and the results are shown in Fig. 5d. The results showed that compared with that in the control group, the expression of the *ACAN* and *COL 2* genes in the 2D-Exo group and the 3D-Exo group was significantly increased, and the 3D-Exo group had the most significant increase. Although there was no significant difference in *Sox9* gene expression between the control group and the 2D-Exo group, there was a significant difference between the 3D-Exo group and the other two groups. The above results indicated that 3D-Exos had a significantly stronger ability than 2D-Exos to promote cartilage formation by BMSCs.

3.6. *Effect of exos on chondrocytes*

To test whether different Exos affect the proliferation of chondrocytes, we performed CCK-8 experiments at different time points. The results showed that on the first day, 2D-Exos and 3D-Exos did not

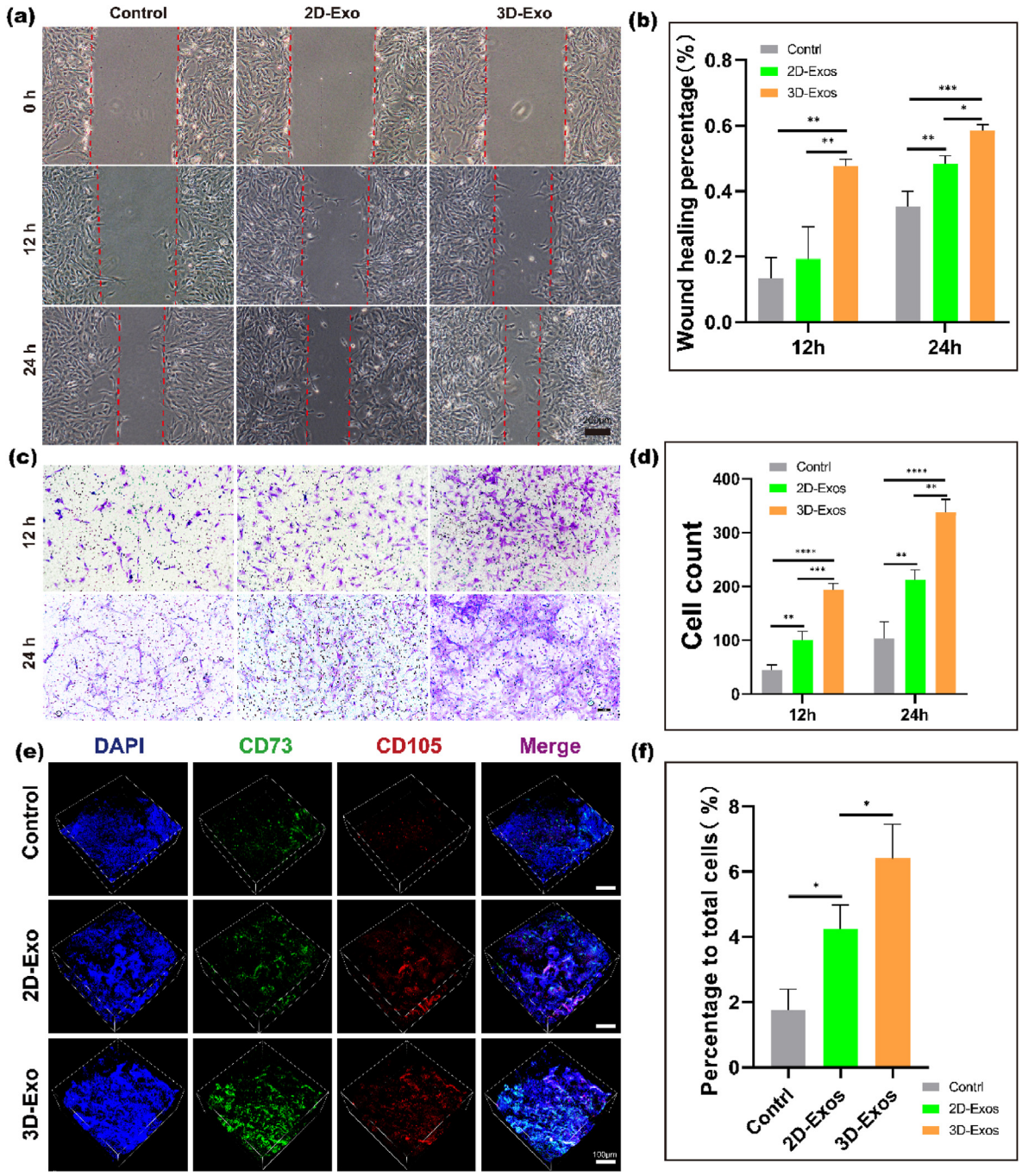

Fig. 4. Effects of different Exos on the migration of BMSCs in vitro and vivo. (a) Images from scratch wound healing experiments after 0 h, 12 h and 24 h. Scale bar = 200 μm. (b) Quantitative analysis of the wound healing percentage of the experiment. Data are presented as the mean ± SD (n = 3). (*P < 0.05, **P < 0.01, ***P < 0.005, ****P < 0.001). (c) Representative images from the Transwell assay after 12 h and 24 h. Scale bar = 10 μm. (d) Quantitative analysis of the cell counts in Transwell assay. (*P < 0.05, **P < 0.01, ***P < 0.005, ****P < 0.001) (n = 3). (e) Confocal 3D images of CD73+/CD105+ MSCs in three groups by immunofluorescence 14days post-surgery and quantification of MSCs that migrated to the site of injury. Scale bar = 100 μm. (f) Quantitative analysis of the data. Data are presented as the mean ± SD (n = 3) (*P < 0.05).

promote the proliferation of chondrocytes compared to the control group. However, on days 3 and 7, both 2D-Exos and 3D-Exos significantly promoted the proliferation of chondrocytes. 3D-Exos promoted the proliferation of chondrocytes significantly better than 2D-Exos, and the two groups were significantly different (Fig. 5g).

The protection of normal chondrocytes in an inflammatory environment is also a very important factor in the process of cartilage repair, so we investigated whether 3D-Exos could protect chondrocytes in an inflammatory environment. IL-1β is a universal inflammatory factor related to induction of an inflammatory response, so we used IL-1β in vitro to mimic the inflammatory microenvironment in vivo. The apoptosis of chondrocytes in different treatment groups was also detected by flow cytometry. As shown in Fig. 5e, chondrocytes underwent significant apoptosis during the IL-1β-induced inflammatory response. 2D-Exo and 3D-Exo treatment inhibited the effect of IL-1β. Compared with 2D-Exos, 3D-Exos inhibited the effect of IL-1β most strongly. Statistical analysis showed that the percentages of apoptotic cells in the control, IL-1β, 2D-Exo and 3D-Exo groups were approximately 7%, 18%, 12% and 9%,

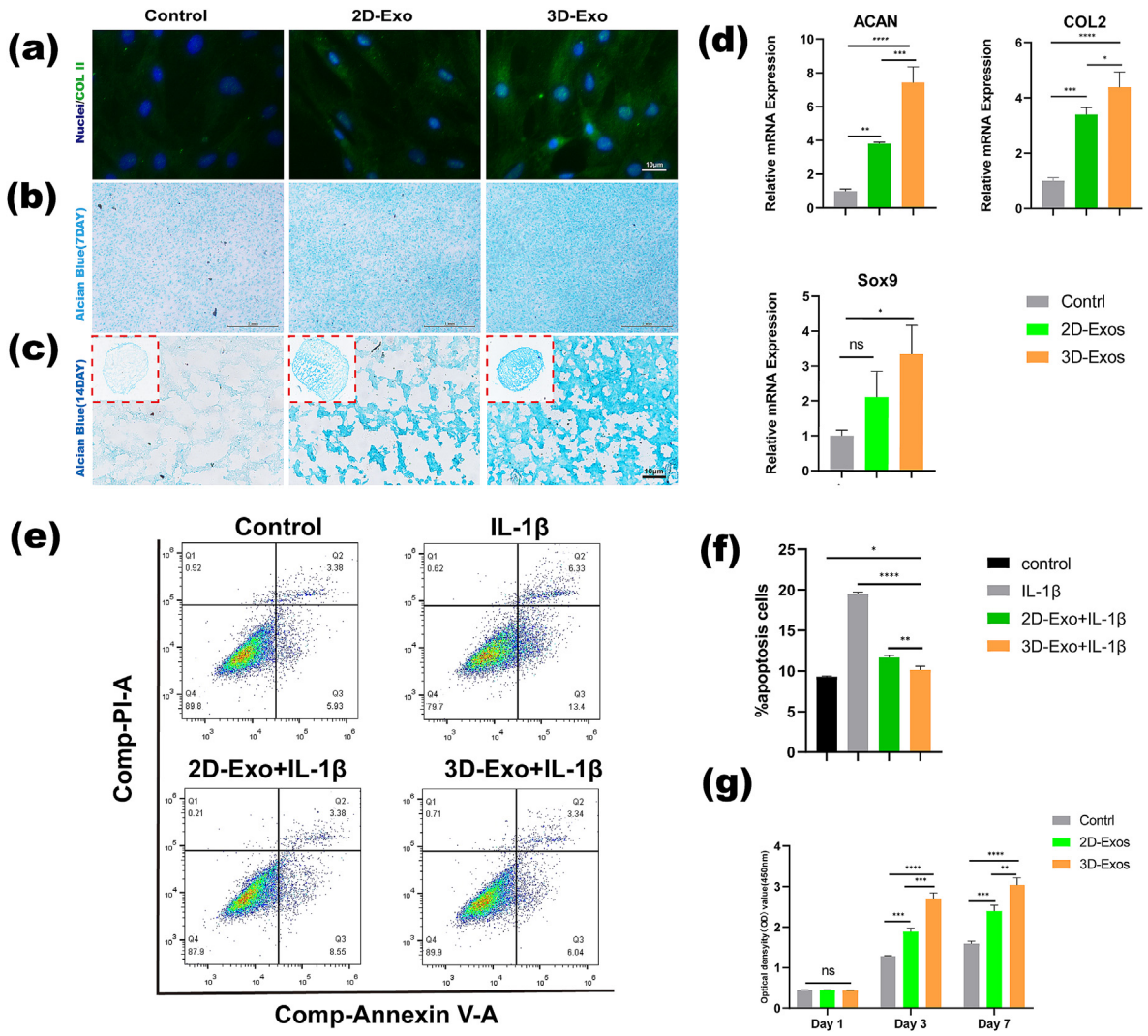

Fig. 5. Comparison of the effects of 3D-Exos and 2D-Exos on the chondrogenic differentiation of BMSCs and chondroprotection. (a) Immunofluorescence images showing the expression of COL II after chondrogenic induction for 7days in BMSCs. Scale bar = 10 μm. (b) Alcian Blue staining for glycosaminoglycan (GAG) accumulation in BMSCs 7 days later. Scale bar = 1 mm. (c) Alcian Blue staining for glycosaminoglycan (GAG) accumulation in BMSC pellets after 14 days. Scale bar = 10 μm. (d) Gene expression of *Col II, Sox9* and *Aggrecan* in BMSCs at **7** days (*P < 0.05, **P < 0.01, ***P < 0.005; ns means no significant difference) (n = 3). (e) Flow cytometry results of the effect of different exosomes on chondrocyte apoptosis in an inflammatory environment. (f) Quantitative analysis of the flow cytometry results. (*P < 0.05, **P < 0.01, ***P < 0.005, ****P < 0.001) (n = 3). (g) CCK-8 assays of the effect of different Exos on chondrocyte viability (**P < 0.01, ***P < 0.005, ****P < 0.001; ns means no significant difference) (n = 3).

respectively (Fig. 5f). The above results suggest that compared with 2D-Exos, 3D-Exos can significantly inhibit apoptosis of chondrocytes in an IL-1β-induced inflammatory environment.

3.7. Immunomodulatory potential of exos

To investigate the effects of 2D-Exos and 3D-Exos on macrophage phenotypic polarization in vitro, we comprehensively analyzed the expression of macrophage-related markers by immunofluorescence staining and RT–qPCR. The results of immunofluorescence staining showed that the expression of CD206 (M2) in the 3D-Exo group was significantly stronger than that in the control and 2D-Exo groups (Fig. 6a). The statistical results showed that the proportion of CD206-positive macrophages in the 3D-Exo group (approximately 36%) was significantly higher than that in the control group (approximately 8%) and the 2D-exo group (approximately 19%) (Fig. 6c). RT–qPCR results showed that the expression of M2 macrophage-related genes *(CD163, Arg-1, and CD206)* in the 3D-Exo group was significantly higher than that in the control group and 2D-Exo group, and the differences were significant (Fig. 6b). Similar results were observed in RAW macrophages, the proportion of CD206 (+)/CD68 (+) macrophages in the 3D-Exo group was significantly higher than other two groups. The above results confirmed that 3D-Exos had the strongest ability to promote the polarization of macrophages to the M2 phenotype, which provided an in vitro basis for future immune regulation approaches in vivo.

We further explored the mechanisms of 3D-Exo in regulating macrophages. Exos downregulated NF-κB p65 expression and reduced its nuclear translocation and reduced the expression of NLRP3 proteins, which is a key pathway for the production of inflammatory factors. (Fig. S3). However, the effect of 3D-Exo treatment was more obvious than that of 2D-Exo, indicating that 3D-Exo might be more efficient than 2D-Exo in immunoregulation. This may be down to the up-regulation of miR-125a and miR-29a (Table 1).

The nuclear factor kappa B (NF-κB) pathway is an essential proinflammatory pathway. Inhibition of the NF-κB pathway could promote the M1-to-M2 switch in macrophages and inactivate the priming signal for the pyrin domain-containing 3 (NLRP3) inflammasome [12]. We found that 3D-Exos downregulated NF-κB expression in macrophages. This

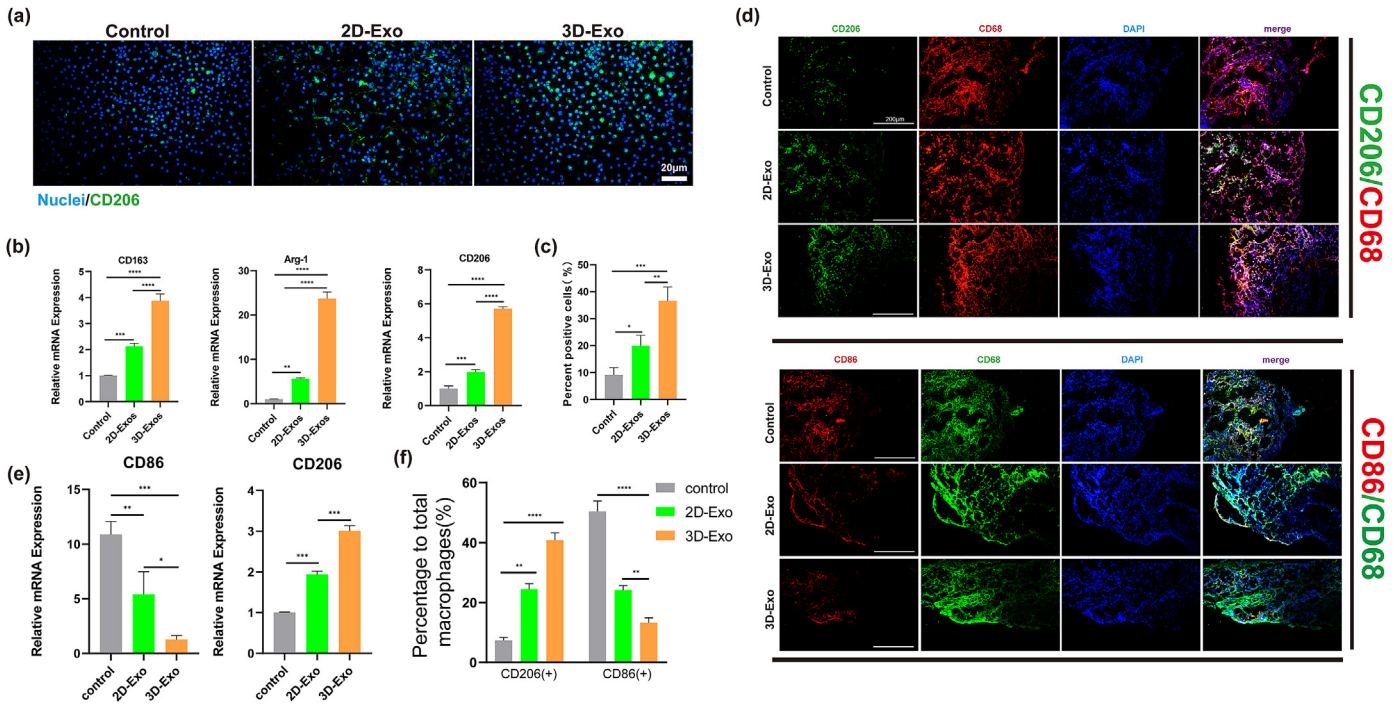

Fig. 6. Evaluation of the polarization ability of macrophages induced by different Exos in vitro and vivo. (a) Immunofluorescence staining of CD206 in macrophages treated with different Exos for 24 h. Scale bar = 20 μm. (b) RT-qPCR detection of M2 ***(CD163、Arg-1、CD206)*** marker gene expression in macrophages cultured with different Exos for 24 h (n = 3). (**P < 0.01, ***P < 0.005). (c) Quantitative analysis of the Im-munofluorescence staining (*P < 0.05, **P < 0.01, ***P < 0.005, ****P < 0.001). N = 3. (d) Immunofluorescence staining of $CD68^{+}$/**CD86**+/$CD206^{+}$ macrophages in synovium at 14 days after surgery. Scale bar = 20 μm. (e) Gene expression of ***CD206*** and ***CD86*** in synovium macrophages at 14 days (*P < 0.05, **P < 0.01, ***P < 0.005) (n = 3). (f) Quantitative analysis of Immunofluorescence staining of $CD86^{+}$/$CD206^{+}$ macrophages in synovium (*P < 0.05, **P < 0.01, ***P < 0.005, ****P < 0.001). N = 3.

Table 1
Differences in miRNAs between 3D-Exos and 2D-Exos.

miRNA	Up/down	Previously reported studies	Ref.
miR-127–5p	up	targets WNT5A, enhances chondrogenesis	[23]
miR-210	up	upregulates Col2 and Sox9 expression , targets Runx3 to promote proliferation, migration	[24,25]
miR-29a-3p	up	upregulates the expression of Sox 9, Col-2a1, and aggrecan , promotes macrophage polarization to the M2 subtype	[26,27]
miR-30a	down	downregulation of Sox9 promotes extracellular matrix degradation	[28]
miR-320	up	targets MMP-13 and regulates chondrogenesis	[29]
miR-328–3p	up	increases chondrocyte viability and attenuates chondrocyte apoptosis and ECM degradation	[30]
miR-574–3p	down	RXRα downregulation	[31]
miR-125a-3p	up	Inhibits TLR and NFκB signaling to switch macrophages to the M2 phenotype	[32]
miR-125a-5p	up	diminishes M1 phenotype expression induced by LPS and promotes M2 marker expression induced by IL-4	[33]
miR-155–5p	down	promotes macrophage M1 polarization and Inhibits polarization of macrophages to the M2 type	[34]
miR-21–5p	Up	reduces apoptosis and promotes macrophage M2 polarization; enhances the proliferation of MSCs	[35–37]
let-7d-3p	down	inhibits intratumoral macrophage M2 polarization	[38]
miR-139–5p	down	targets IGF-1R to inhibit proliferation and migration	[39]

effect could explain the decrease in NLRP3, as NF-κB is an upstream signal of NLRP3. In summary, 3D-Exos could promote M2 polarization by inhibiting the activation of inflammasomes, thus creating a pro-regenerative immune microenvironment.

3.8. *In vivo animal experiment*

3.8.1. *Biodistribution of exos*

To observe the morphology of 3D-Exos on the scaffolds, we performed SEM. The SEM results showed (Fig. S1b) that 3D-Exos were able to get inside the scaffold, fuse well with the scaffold, and retain the morphological characteristics of Exos.

To evaluate the adsorption effect of the scaffold on Exos, we labeled 3D-Exo with DiO, loaded 3D-Exos on the scaffold in vitro, and finally implanted the scaffold loaded with 3D-Exos into knee cartilage defects in mice. Joint cavity injection of Dio-labeled 3D-Exos alone served as the control group. After 48 h, the mice were sacrificed and stained for observation. The results are shown in Fig. S1a. Injection of Dio-labeled 3D-Exos alone resulted in substantial loss in the joint cavity, and no significant enrichment was seen at the defect. However, a large number of Exos (green fluorescence) were still seen in the scaffold group loaded with 3D-Exos and were present in the defect.

Two groups (the free exosome group and the exosome-loaded scaffold group) were placed in situ in cartilage defects to assess the retention time of exosomes within the joint. In vivo imaging showed that the fluorescence of the exosome injection group nearly disappeared within 3 days. After incorporation of Exos into the scaffolds, the fluorescence remained on the third day and disappeared over 5 days. (Fig. S1.c)

3.8.2. Regulatory effect of exos on the articular cavity microenvironment

To further explore the mechanism of inflammation regulation by 3D-Exos, we performed immunofluorescence staining and RT-qPCR analysis (Fig. 6d and e) of CD68, CD86 and CD206, specific markers of all M0/M1/M2 macrophages in the synovial membrane, to compare the effects of 3D-Exos and 2D-Exos on macrophage polarization. The results showed that the expression of CD206 in the 3D-Exos group was significantly higher than that in the control and 2D-Exo groups on the 14th day. The expression of CD86 in the control and 2D-Exo groups was significantly higher than that in the 3D-Exo groups. The statistical results in Fig. 6f show that the percentage of CD206 positive macrophage was significantly higher in the 3D-Exo groups (approximately 40%) than in the control groups (approximately 9%) and 2D-Exo groups (approximately 22%) and the difference was significant. The percentage of CD86-positive macrophages was significantly lower in the 3D-Exo groups (approximately 11%) than in the control groups (approximately 49%) and 2D-Exo groups (approximately 23%) and the RT–qPCR results showed that 3D-Exos significantly promoted the expression of an M2-associated gene (*CD206*) and suppressed the expression of an M1-associated gene (*CD86*) compared to 2D-Exos (Fig. 6e). The above results showed that 3D-Exos promoted macrophage polarization toward the M2 phenotype and had the strongest anti-inflammatory effect in vivo.

3.8.3. Exosomes and scaffolds' immune response in rats

Acute inflammatory and immune responses to the scaffold and Exosomes were observed at 1 week after subcutaneous implantation in rats. No obvious scar tissues formation was found around the implants in the H&E staining images. We observed a small amount of neutrophil and monocyte infiltration around the scaffold, suggesting that the implants had appropriate immunogenic properties. Few immune cells was observed at the injection site (Fig.S2.e), which is consistent with the previous study about the low-immunogenicity of exosomes [13].

3.8.4. Reparative effect of exos on osteochondral defects

To investigate whether 3D-Exos combined with ECM scaffolds could promote osteochondral regeneration, we established a rat articular osteochondral defect model (2.0 mm in diameter and 1.0 mm in depth). The rats were randomly divided into 5 groups of 6 rats each groups, as shown in Fig. 7f. Images of the cartilage regeneration area at 4 and 8 weeks after surgery are shown in Fig. 7a. At 4 weeks, the cartilage defect in the control group was still obvious, with only a small amount of granulation tissue, a rough surface and a clear boundary with the surrounding cartilage. The repaired tissue in the 2D-Exo group, 3D-Exo group and scaffold group had a significantly greater height than that in the control group, but it was still thinner than the surrounding normal cartilage, and the shape of the repaired surface was still uneven. The repaired tissue in the 3D-Exo group had mostly filled the cartilage defect area, but the surface was uneven, and there was still a demarcation between the new tissue and the normal cartilage. There was a large amount of repaired tissue in the cartilage defect in the control group at 8 weeks, but the cartilage was distinct from the surrounding normal cartilage. The repaired tissues in the 2D-exo group and 3D-exo group had largely filled the cartilage defect area, but the surface was uneven, and there was still a demarcation between the new tissue and the normal cartilage. In the

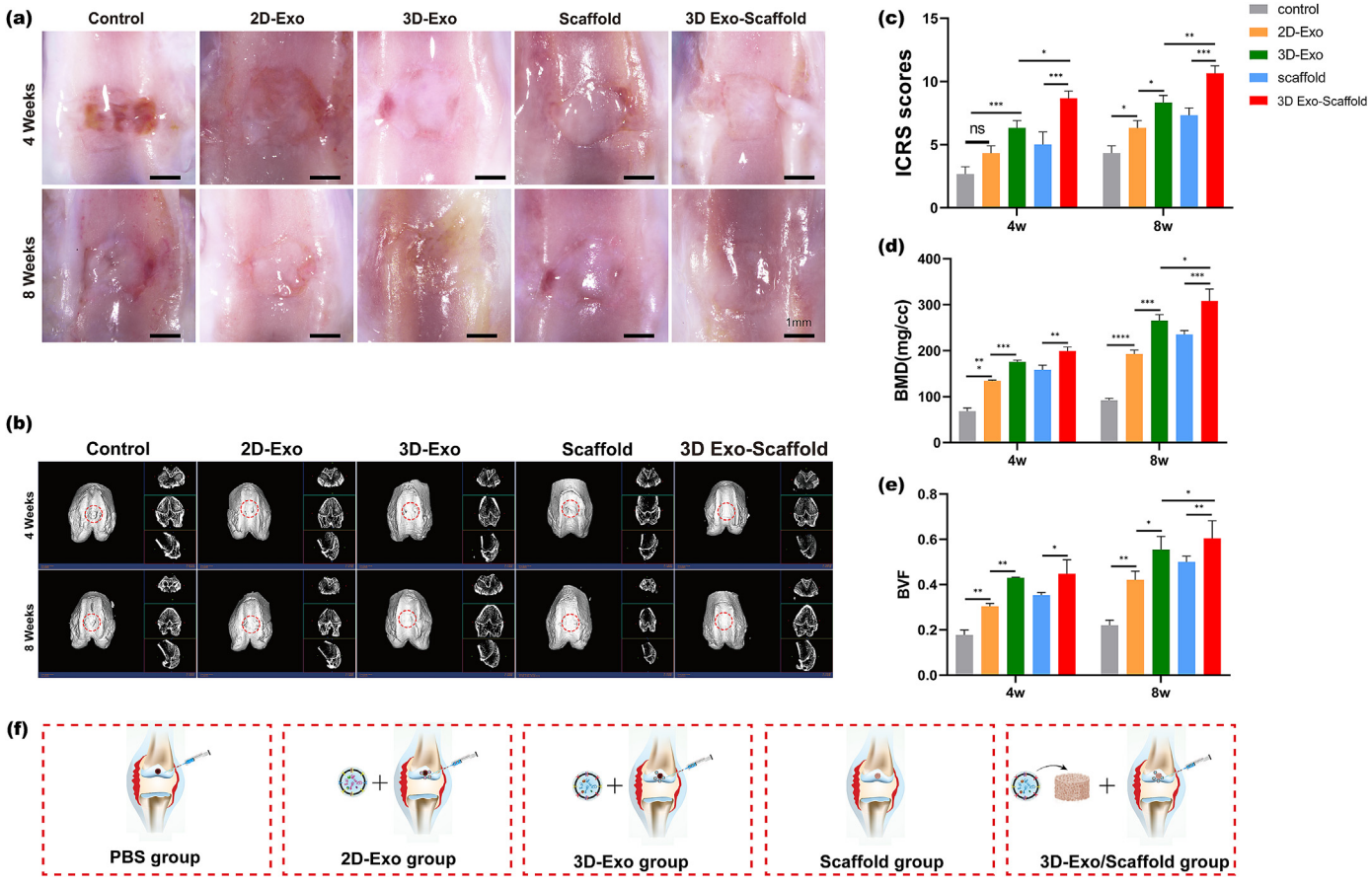

Fig. 7. (a) Microscopic observation of the repaired tissues at 4 weeks and 8 weeks. Scale bar = 1 μm. (b) Micro-CT images showing 2D and 3D reconstructions of the repaired cartilage. (c) ICROS score of the cartilage defect after 4 and 8 weeks. (*P < 0.05, **P < 0.01, ***P < 0.005, ****P < 0.001, ns means no significant difference). n = 3. (*d*–e) Quantitative analysis of BMD and BV/TV in the defect area (*P < 0.05, **P < 0.01). N = 3. (f) Schematic diagram of the experimental group designed in vivoSchematic diagram of the experimental group designed in vivo.

scaffold group, the new tissue was smooth, and the border with the surrounding tissue was not obvious, but there was a significant difference in color between the new tissue and normal cartilage. The ICRS score (Fig. 7c) also showed significantly better cartilage repair in the 3D-exo/ECM group at 4 and 8 weeks than in the other groups.

The results of regenerative defect repair in the five groups were compared by micro-CT analysis (Fig. 7b). 2D and 3D reconstructions of femoral specimens at 4 and 8 weeks were analyzed to evaluate bone mineral density (BMD) and bone volume/tissue volume (BV/TV), which are important indicators of subchondral bone (Fig. 7d and e). Morphogenetic analysis showed that the 3D-Exo + scaffold group had significantly more repaired tissue than the other four groups (the 2D-Exo group, 3D-Exo group, and scaffold group) at 4 and 8 weeks postoperatively, and the differences were statistically significant. In the 3D-Exo + scaffold group, cartilage-like tissue was formed at 8 weeks postoperatively, and the defect almost completely disappeared. In addition, the 3D-Exo + scaffold group had significantly higher bone density values than the other groups (the 2D-Exo group, 3D-Exo group, and scaffold group), which indicated an increase in the amount of tissue repair in the defect. Consistent with the BMD results, the BV/TV assessment showed a significant increase in the 3D-Exo + scaffold group at 4 and 8 weeks after surgery.

The cartilage defect areas were evaluated by HE, safranin-O/Fast Green, Sirius Red, and COL II immunohistochemical staining. At 4 weeks postoperatively (Fig. 8a), no obvious signs of repair were observed in the cartilage defect area in the control group, the boundary between the repaired area and the normal tissue was clear, and the thickness of the cartilage in the repair area was smaller than that in normal tissue. The cartilage defect area in the 2D-exo group and scaffold group was disorganized and filled with irregular fibrous tissue, and the expression of glycans and COL II was low. In addition, the boundary between normal cartilage and the repaired area was obvious. There was partial chondrocyte formation in the repaired area in the 3D-exo group, but there were fissures between the normal tissue and the regenerated area, and flocculent fibrous tissue was also visible on the surface. There was still a small amount of fibrous tissue on the surface of the defect area in the 3D-Exo + scaffold group, but the defect area had largely fused with the normal tissue, and the thickness of the defect area was close to that of the normal area. The number of chondrocytes increased, and there was abundant expression of glycans and COL II in the 3D-Exo + scaffold group. At 8 weeks (Fig. 8b), protruding fibrous tissue was still visible in the repaired area in the control group. In the 2D-Exo group and the scaffold group, chondrocytes appeared in the repaired area but were disordered. The repaired area was basically fused with the normal area, but the interface was clearly visible in the 2D-Exo group and the scaffold group. In the 3D-exo group, there were obvious cartilage gaps, but they were not neatly aligned. The glycan and COL II levels in the 3D-Exo group were increased compared with those in the 2D-Exo group and the scaffold group. In the 3D-Exo + scaffold group, the repaired area resembled normal tissue, with a large number of chondrocytes and relatively normal alignment, and there was significantly enhanced expression of glycans and COL II. The results of MODHS (Fig. 8c) and COL II semiquantitative scores (Fig. 8d) also confirmed that the best osteochondral repair effect was achieved in the 3D-Exo + scaffold group.

In general, histologically, the 3D-Exo + scaffold group showed more complete repair than the other groups (the control group, 2D-Exo group, 3D-Exo group, and scaffold group).

3.9. Differences in miRNAs between 3D-Exos and 2D-Exos and bioinformatics analysis

A large number of miRNAs encapsulated in Exos are capable of posttranscriptional regulation of coding genes and are recognized as critical for influencing the biological activity of recipient cells, which has become an important direction for Exo research in recent years. To further investigate the effects of 3D scaffold culture on miRNAs in Exos, miRNA microarray analysis was performed to detect miRNA expression in two groups of Exos, and GO and KEGG analyses were performed to investigate the biological processes, specific molecular functions and related signaling pathways associated with differentially expressed miRNAs. A total of 116 miRNAs with significant differences were detected between 3D-Exos and 2D-Exos. We identified miRNAs with significant differences, of which 59 were upregulated and 57 were downregulated (Fig. 9a), indicating differences in the intrinsic composition of Exos within stem cells from different culture sources. We enumerated 13 miRNAs that may be associated with cartilage injury repair, including negative regulation of apoptosis, promotion of cell proliferation, promotion of stem cell chondrogenic differentiation, and promotion of macrophage to M2 transformation (Table 1). KEGG pathway analysis showed that the differentially expressed miRNAs were involved in the Rap1 signaling pathway, cAMP signaling pathway, TGF-β signaling pathway (10) and Wnt signaling pathway. GO analysis of target genes showed that the important biological processes included positive regulation of stem cell differentiation, positive regulation of chondrogenesis, macrophage activation in stem cells and chondrocyte proliferation and immune response (Fig. 9b–d). The important molecular functions included beta-catenin binding, MAP kinase activity, collagen binding, chondroitin sulfate binding and growth factor receptor. Based on pathway enrichment analysis, these miRNAs in 3D-Exos are hypothesized to be essential for cellular behavior, cell determination and immune regulation.

4. Discussion

Cartilage repair after injury has long been a challenge for clinicians. There are many treatment methods for cartilage injury, among which stem cell therapy has recently attracted much attention, and numerous studies have shown that stem cell therapy contributes to cartilage injury repair. However, stem cell therapy has some limitations: 1. Strict conditions for the storage and transportation of stem cells; 2. A risk of tumorigenicity and disease transmission by stem cells; and 3. Possible immune rejection of stem cell therapy [14,15]. It has been shown that stem cells perform their biological functions mainly through paracrine secretion. Exos have been widely investigated because of their role in intercellular communication and their potential in the treatment of diseases [16–18]. Exos, as products of stem cell paracrine secretion, are rich in bioactive molecules (miRNAs, proteins, lncRNAs, etc.) and function in cell-to-cell communication. Exos overcome the abovementioned limitations of stem cell therapy and promote tissue repair and regeneration. Most Exos are derived from 2D-cultured cells, but traditional 2D culture does not resemble the natural microenvironment of MSCs. There is increasing evidence that 3D culture models can better simulate the microenvironment in vivo. The biological behavior of cells on 3D scaffolds differs from that of cells in conventional 2D culture, and 3D scaffold culture can more realistically simulate cell–cell and cell-matrix interactions [19], which can enhance the paracrine function of mesenchymal stem cells (MSCs). It was reported that 3D-Exos were able to promote spinal cord repair [19]. Yang et al. found that 3D cultured hUMSC-derived Exos could be used to treat Alzheimer's disease (AD) [20]. The above findings suggest that 3D-Exos can promote tissue repair.

This experiment investigated the differences in cartilage repair between Exos derived from 2D culture and 3D culture. First, we compared the differences between 2D ECM films and 3D scaffolds, as well as hUMSCs grown under such conditions. The results showed that compared with 2D ECM films, 3D scaffolds not only have a distinct 3D structure with sparse, highly interconnected micropores but also have micrometer-scale morphological features, and this structure can promote communication between stem cells and facilitate stem cell paracrine function. hUMSCs were incubated under the above culture conditions separately, and it was found that the hUMSCs were more active on the 3D scaffolds. It was also found that the 3D scaffolds could enhance the attachment and diffusion of hUMSC and provide more surface area for

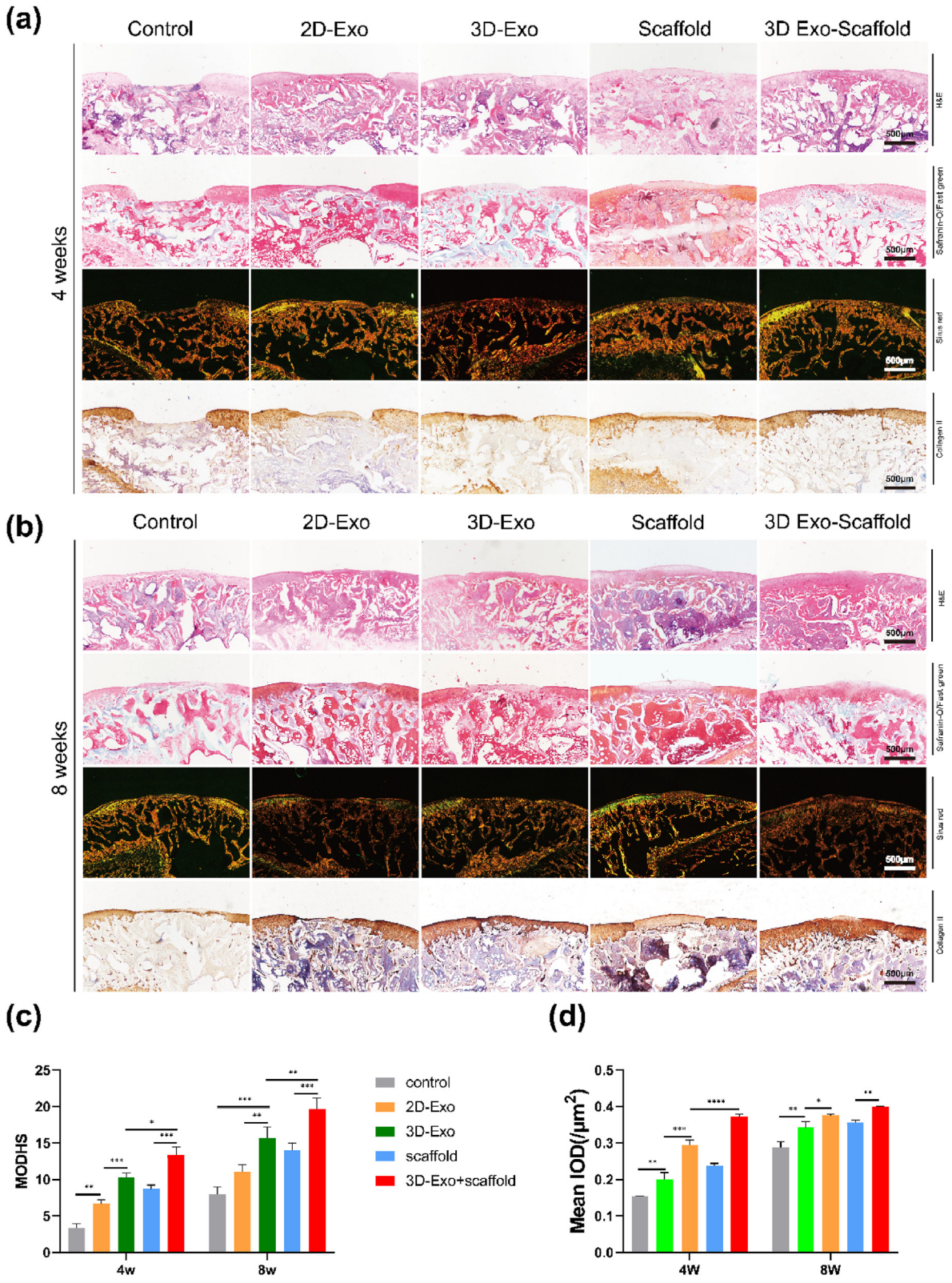

Fig. 8. Histological evaluation of in vivo cartilage regeneration after 4 and 8 weeks. (a,b) H&E, safranin-O, and Sirius red staining and immunohistochemical staining of COL II of repaired tissue in different groups after 4 and 8 weeks. Scale bar = 500 μm. (c) MODHS histological evaluations of repaired tissue (n = 3) (**P < 0.01, ***P < 0.005). (d) Quantitative analysis of COL II was performed (n = 3) (*P < 0.05, **P < 0.01, ***P < 0.005, ****P < 0.001).

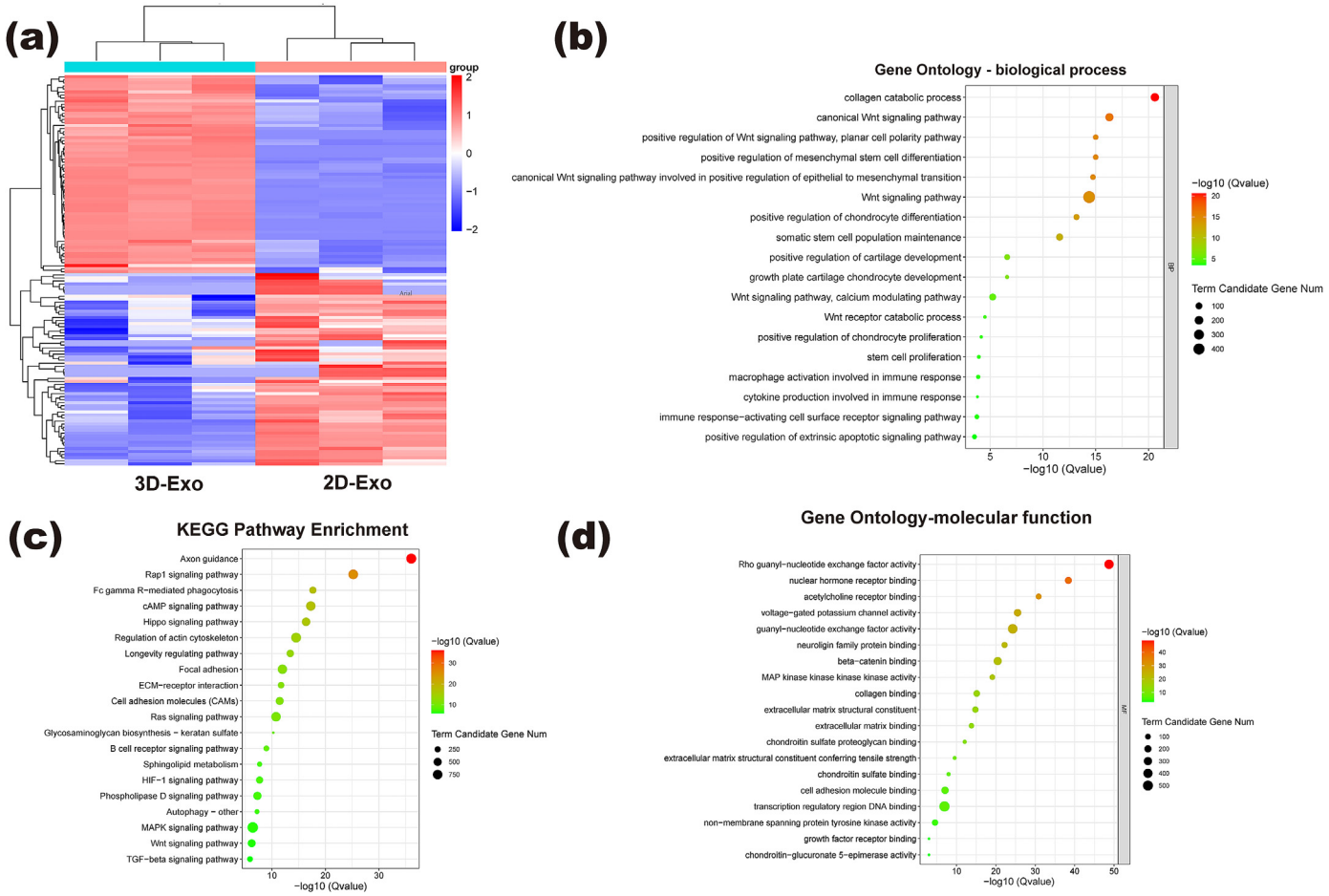

Fig. 9. GO and KEGG analyses of miRNA target genes of different Exos: (a) Microarray analysis of exosomal miRNAs is presented in a heatmap. (b,d) GO analyses including biological process and molecular function; (c) KEGG pathway enrichment.

the growth of hUMSCs, which is consistent with previous studies [9]. In terms of paracrine function, the size of individual pores plays an integral role in regulating cellular responses, and high porosity increases the distance between cells. Cells in such conditions may need to release more Exos or rely on special cargo for intercellular communication. Articular cavity-resident MSCs play a dominant role in cartilage injury repair, and an ideal regenerative microenvironment promotes the repair-related biological functions of MSCs, such as proliferation, migration, and chondrogenic differentiation. The most common approach to improving the regenerative microenvironment has been the use of various chemotactic agents, such as transforming growth factor-β3 (TGF-β3), but most chemotactic agents have a single function and cannot fully regulate the biological function of MSCs. Here, we attempted to regulate the biological functions of BMSCs with Exos instead of traditional chemotactic agents to improve the regenerative microenvironment. First, we extracted and characterized exosomes that were cultured under different culture conditions. The results showed that we successfully extracted exosomes. The obtained 2D-Exos and 3D-Exos differed in size, with 3D-Exos being significantly smaller than 2D-Exos. Both exosomes expressed exosome-specific proteins. The ability of exosomes (2D-Exo, 3D-Exo) to enter the cell is a prerequisite for their function, and we have shown that BMSCs and macrophages are able to take up Exos. Additionally, in vivo distribution data showed that mixing 3D-Exos into the scaffold could restrict the exosomes to the defect site and avoid massive loss. We next investigated the effect of 3D-Exos on the proliferation of BMSCs. The results of the proliferation assay showed that 3D-Exos significantly promoted the proliferation of BMSCs by promoting the shift from the G1 to S phase of the cell cycle compared to 2D-Exos. The migration of BMSCs plays a decisive role in cartilage repair. For the in vitro migration assay, we used scratch assays and Transwell assays to explore the different effects of 2D-Exos and 3D-Exos on the migration of BMSCs. The experimental results showed that 3D-Exos promoted the migration of BMSCs significantly better than 2D-Exos. Then, we used a rat osteochondral defect model to evaluate the effect of 2D-Exos and 3D-Exos on stem cell migration in vivo. The results showed that joint cavity injection of 3D-Exos significantly improved the migration ability of endogenous stem cells in the joint cavity. In this experiment, we also investigated the effect of 3D-Exos on the chondrogenic differentiation of BMSCs by different experimental methods. The results showed that 3D-Exos promoted the chondrogenic differentiation of BMSCs better than 2D-Exos. In recent years, immunomodulatory capacity has been considered an important factor affecting tissue regeneration, and the effectiveness of early active regulation of macrophages by stimulants in tissue repair has been confirmed. The role of macrophages in cartilage regeneration has received increasing attention. M1-type macrophages secrete proinflammatory factors and are involved in tissue destruction, whereas M2-type macrophages play an important role in the response to tissue remodeling, and how to regulate the polarization of macrophages to M2-type macrophages in the joint cavity is seen as an important research direction for cartilage regeneration. Both in vivo and in vitro experimental data have confirmed that 3D-Exo might be more efficient than 2D-Exo in immunoregulation. The immunomodulatory effect of 3D-Exo protects normal chondrocytes from apoptosis in the inflammatory environment. In vitro anti-apoptotic assays have demonstrated the chondroprotective effect of 3D-Exo.

miRNAs are small noncoding RNAs that regulate gene expression by

recognizing homologous sequences and interfering with transcriptional, translational, or epigenetic processes [16]. MiRNA sequencing and analysis showed that miRNAs in 3D-Exos can promote cartilage matrix synthesis and cartilage regeneration. Furthermore, by target gene prediction, we identified miRNAs with beneficial effects on regulating the joint cavity microenvironment (**Table 1**). Functional enrichment analysis of high-abundance miRNAs based on total read counts identified the most important biological signaling pathways. This narrowed the scope to further define the molecular mechanisms of 3D-Exos in cartilage repair and provided a reference to identify new regulatory targets for cartilage regeneration. A preliminary explanation of the possible mechanism for the superiority of 3D-Exo over 2D-Exo in cartilage repair was provided by miRNA sequencing.

Notably, the current evidence relies on interesting in vitro data, and convincing data need to be generated in a rat model of osteochondral defects. Therefore, to elucidate the role of 2D-Exos and 3D-Exos in repairing osteochondral defects in vivo, we performed in vivo experiments. The experiment was divided into five groups: the PBS group, 2D-Exo group, 3D-Exo group, scaffold group, and 3D-Exo group/scaffold group, along with sequential postoperative intra-articular cavity injection of exosomes. Compared with the 2D-Exo group, the 3D-Exo group had higher Col II content and obvious cartilage gaps in the eighth week after surgery, indicating that 3D-Exos are more advantageous than 2D-Exos in tissue repair. Since local injection of exosomes did not guarantee their retention in the injury area, 3D-Exos and stents were combined in this experiment. In addition, the scaffolds facilitate cell spreading, migration and the establishment of a macroporous microenvironment for intercellular contact [22]. To keep the exosomes active and maintain their repair effect in vivo, we injected exosomes into the joint cavity at 5-day intervals. Samples were collected at 4 and 8 weeks postoperatively and subsequently evaluated by gross observation, micro-CT assays, and histological staining, and the results showed that the 3D-Exo group/scaffold group had a significantly better repair effect than the other groups (the PBS group, 2D-Exo group, 3D-Exo group, and scaffold group).

Although the above experiments and studies clearly demonstrate that 3D-Exos combined with scaffolds can greatly improve the quality of cartilage regeneration, there are still some limitations that need to be discussed. (1) In vivo experiments, Exos were continuously injected once every 5 days after surgery, which increased the risk of intra-articular infection. Scaffold which is more suitable for exosomes deliverying still need to be explored. (2) The metabolism of Exos in vivo still needs to be further explored. (3) The exact duration for which the biological activity of exosomes can be maintained in vivo still needs to be further investigated. (4) Although we found differences in miRNA expression between 2D-Exos and 3D-Exos, it is not clear which miRNA plays a central role. The downstream mechanisms of related biological functions still need to be further explored.

5. Conclusion

Our results show that the biological function of exosomes is influenced by different culture conditions. In vitro data showed that 3D-Exos better promoted the proliferation, migration and chondrogenic differentiation of BMSCs than 2D-Exos. Additionally, both in vitro and in vivo data confirmed that 3D-Exos better attenuated inflammation and promoted macrophage polarization toward the M2 phenotype. The differences in miRNAs between 2D-Exos and 3D-Exos were evaluated by miRNA sequencing, and the results showed that miRNAs related to cartilage repair were significantly upregulated in 3D-Exos, which tentatively explained the superior effects of 3D-Exos over 2D-Exos in cartilage repair. Moreover, the results of in vivo experiments showed that 3D-Exos combined with scaffolds could repair osteochondral defects well. This study provides insights into a new therapeutic intervention and the potential clinical application of Exos derived from hUMSCs cultured on 3D scaffolds in the treatment of cartilage injury, in addition to demonstrating the efficacy and safety of this approach.

Credit author statement

ZNY, MXC, SYL and QYG conceived and designed the experiments. ZNY, HY and JW conducted the experiments. GZT, MZL, ZYL, SLH, HYD analyzed the results. ZNY, HY and JW wrote the manuscript. CN, ZGD, XY, XS and SYL reviewed the manuscript. All authors read and approved the final manuscript.

Declaration of competing interest

The authors declare that they have no known competing financial interests or personal relationships that could have appeared to influence the work reported in this paper.

Data availability

No data was used for the research described in the article.

Acknowledgments

This study was supported by the National Key R&D Program of China (2019YFA0110600).

Appendix A. Supplementary data

Supplementary data to this article can be found online at https://doi.org/10.1016/j.mtbio.2023.100549.

References

[1] P. Wang, Q. Meng, W. Wang, S. Zhang, X. Xiong, S. Qin, J. Zhang, A. Li, Z. Liu, Icariin inhibits the inflammation through down-regulating NF-kappaB/HIF-2alpha signal pathways in chondrocytes, Biosci. Rep. (2020) 40.
[2] J. Sellam, F. Berenbaum, The role of synovitis in pathophysiology and clinical symptoms of osteoarthritis, Nat. Rev. Rheumatol. 6 (2010) 625–635.
[3] G. Tian, S. Jiang, J. Li, F. Wei, X. Li, Y. Ding, Z. Yang, Z. Sun, K. Zha, F. Wang, B. Huang, L. Peng, Q. Wang, Z. Tian, X. Yang, Z. Wang, Q. Guo, W. Guo, S. Liu, Cell-free decellularized cartilage extracellular matrix scaffolds combined with interleukin 4 promote osteochondral repair through immunomodulatory macrophages: in vitro and in vivo preclinical study, Acta Biomater. 127 (2021) 131–145.
[4] D. Kouroupis, D. Correa, Increased mesenchymal stem cell functionalization in three-dimensional manufacturing settings for enhanced therapeutic applications, Front. Bioeng. Biotechnol. 9 (2021), 621748.
[5] L. Qing, H. Chen, J. Tang, X. Jia, Exosomes and their MicroRNA cargo: new players in peripheral nerve regeneration, Neurorehabilitation Neural Repair 32 (2018) 765–776.
[6] E.S. Kim, K. Kida, J. Mok, Y. Seong, S.Y. Jo, T. Kanaki, M. Horikawa, K.H. Kim, T.M. Kim, T.S. Park, J. Park, Cellhesion VP enhances the immunomodulating potential of human mesenchymal stem cell-derived extracellular vesicles, Biomaterials 271 (2021), 120742.
[7] S. Rocha, J. Carvalho, P. Oliveira, M. Voglstaetter, D. Schvartz, A.R. Thomsen, N. Walter, R. Khanduri, J.C. Sanchez, A. Keller, C. Oliveira, I. Nazarenko, 3D cellular architecture affects MicroRNA and protein cargo of extracellular vesicles, Adv. Sci. 6 (2019), 1800948.
[8] O. Habanjar, M. Diab-Assaf, F. Caldefie-Chezet, L. Delort, 3D cell culture systems: tumor application, advantages, and disadvantages, Int. J. Mol. Sci. 2021 (2021) 22.
[9] M. Chen, Y. Li, S. Liu, Z. Feng, H. Wang, D. Yang, W. Guo, Z. Yuan, S. Gao, Y. Zhang, K. Zha, B. Huang, F. Wei, X. Sang, Q. Tian, X. Yang, X. Sui, Y. Zhou, Y. Zheng, Q. Guo, Hierarchical macro-microporous WPU-ECM scaffolds combined with microfracture promote in situ articular cartilage regeneration in rabbits, Bioact. Mater. 6 (2021) 1932–1944.
[10] S. Jiang, G. Tian, Z. Yang, X. Gao, F. Wang, J. Li, Z. Tian, B. Huang, F. Wei, X. Sang, L. Shao, J. Zhou, Z. Wang, S. Liu, X. Sui, Q. Guo, W. Guo, X. Li, Enhancement of acellular cartilage matrix scaffold by Wharton's jelly mesenchymal stem cell-derived exosomes to promote osteochondral regeneration, Bioact. Mater. 6 (2021) 2711–2728.
[11] M. Lian, B. Sun, Y. Han, B. Yu, W. Xin, R. Xu, B. Ni, W. Jiang, Y. Hao, X. Zhang, Y. Shen, Z. Qiao, K. Dai, A low-temperature-printed hierarchical porous sponge-like scaffold that promotes cell-material interaction and modulates paracrine activity of MSCs for vascularized bone regeneration, Biomaterials 274 (2021), 120841.

[12] L. Xiao, H. Zheng, J. Li, Q. Wang, H. Sun, Neuroinflammation mediated by NLRP3 inflammasome after intracerebral hemorrhage and potential therapeutic targets, Mol. Neurobiol. 57 (2020) 5130–5149.
[13] Y. Yaghoubi, A. Movassaghpour, M. Zamani, M. Talebi, A. Mehdizadeh, M. Yousefi, Human umbilical cord mesenchymal stem cells derived-exosomes in diseases treatment, Life Sci. 233 (2019), 116733.
[14] Z. Veceric-Haler, A. Cerar, M. Perse, (Mesenchymal) stem cell-based therapy in cisplatin-induced acute kidney injury animal model: risk of immunogenicity and tumorigenicity, Stem Cell. Int. 2017 (2017), 7304643.
[15] L. Barkholt, E. Flory, V. Jekerle, S. Lucas-Samuel, P. Ahnert, L. Bisset, D. Buscher, W. Fibbe, A. Foussat, M. Kwa, O. Lantz, R. Maciulaitis, T. Palomaki, C.K. Schneider, L. Sensebe, G. Tachdjian, K. Tarte, L. Tosca, P. Salmikangas, Risk of tumorigenicity in mesenchymal stromal cell-based therapies–bridging scientific observations and regulatory viewpoints, Cytotherapy 15 (2013) 753–759.
[16] Z. Li, S. Hu, K. Cheng, Chemical engineering of cell therapy for heart diseases, Acc. Chem. Res. 52 (2019) 1687–1696.
[17] L. Qiao, S. Hu, S. Liu, H. Zhang, H. Ma, K. Huang, Z. Li, T. Su, A. Vandergriff, J. Tang, T. Allen, P.U. Dinh, J. Cores, Q. Yin, Y. Li, K. Cheng, microRNA-21-5p dysregulation in exosomes derived from heart failure patients impairs regenerative potential, J. Clin. Invest. 129 (2019) 2237–2250.
[18] A.C. Vandergriff, J.B. de Andrade, J. Tang, M.T. Hensley, J.A. Piedrahita, T.G. Caranasos, K. Cheng, Intravenous cardiac stem cell-derived exosomes ameliorate cardiac dysfunction in doxorubicin induced dilated cardiomyopathy, Stem Cell. Int. 2015 (2015), 960926.
[19] M. Han, H. Yang, X. Lu, Y. Li, Z. Liu, F. Li, Z. Shang, X. Wang, X. Li, J. Li, H. Liu, T. Xin, Three-dimensional-cultured MSC-derived exosome-hydrogel hybrid microneedle array patch for spinal cord repair, Nano Lett. 22 (2022) 6391–6401.
[20] L. Yang, Y. Zhai, Y. Hao, Z. Zhu, G. Cheng, The regulatory functionality of exosomes derived from hUMSCs in 3D culture for Alzheimer's disease therapy, Small 16 (2020), e1906273.
[22] T.H. Qazi, D.J. Mooney, G.N. Duda, S. Geissler, Biomaterials that promote cell-cell interactions enhance the paracrine function of MSCs, Biomaterials 140 (2017) 103–114.
[23] G. Mao, Z. Zhang, S. Hu, Z. Zhang, Z. Chang, Z. Huang, W. Liao, Y. Kang, Exosomes derived from miR-92a-3p-overexpressing human mesenchymal stem cells enhance chondrogenesis and suppress cartilage degradation via targeting WNT5A, Stem Cell Res. Ther. 9 (2018) 247.
[24] M. Yang, X. Yan, F.Z. Yuan, J. Ye, M.Z. Du, Z.M. Mao, B.B. Xu, Y.R. Chen, Y.F. Song, B.S. Fan, J.K. Yu, MicroRNA-210-3p promotes chondrogenic differentiation and inhibits adipogenic differentiation correlated with HIF-3alpha signalling in bone marrow mesenchymal stem cells, BioMed Res. Int. 2021 (2021), 6699910.
[25] Z. Zheng, L. Liu, Y. Zhan, S. Yu, T. Kang, Adipose-derived stem cell-derived microvesicle-released miR-210 promoted proliferation, migration and invasion of endothelial cells by regulating RUNX3, Cell Cycle 17 (2018) 1026–1033.
[26] Q. Wang, Y. Chen, X. Shen, J. Chen, Y. Li, Intra-articular injection of miR-29a-3p of BMSCs promotes cartilage self-repairing and alleviates pain in the rat osteoarthritis, Tissue Eng Regen Med 18 (2021) 1045–1055.
[27] J. Cai, B. Qiao, N. Gao, N. Lin, W. He, Oral squamous cell carcinoma-derived exosomes promote M2 subtype macrophage polarization mediated by exosome-enclosed miR-29a-3p, Am. J. Physiol. Cell Physiol. 316 (2019) C731–C740.
[28] T. Chang, J. Xie, H. Li, D. Li, P. Liu, Y. Hu, MicroRNA-30a promotes extracellular matrix degradation in articular cartilage via downregulation of Sox9, Cell Prolif 49 (2016) 207–218.
[29] F. Meng, Z. Zhang, W. Chen, G. Huang, A. He, C. Hou, Y. Long, Z. Yang, Z. Zhang, W. Liao, MicroRNA-320 regulates matrix metalloproteinase-13 expression in chondrogenesis and interleukin-1beta-induced chondrocyte responses, Osteoarthritis Cartilage 24 (2016) 932–941.
[30] J. Yang, M. Zhang, D. Yang, Y. Ma, Y. Tang, M. Xing, L. Li, L. Chen, Y. Jin, C. Ma, m(6)A-mediated upregulation of AC008 promotes osteoarthritis progression through the miR-328-3pAQP1/ANKH axis, Exp. Mol. Med. 53 (2021) 1723–1734.
[31] D. Guerit, D. Philipot, P. Chuchana, K. Toupet, J.M. Brondello, M. Mathieu, C. Jorgensen, D. Noel, Sox9-regulated miRNA-574-3p inhibits chondrogenic differentiation of mesenchymal stem cells, PLoS One 8 (2013), e62582.
[32] J. Zheng, Y. Kong, X. Hu, Z. Li, Y. Li, Y. Zhong, X. Wei, J. Ling, MicroRNA-enriched small extracellular vesicles possess odonto-immunomodulatory properties for modulating the immune response of macrophages and promoting odontogenesis, Stem Cell Res. Ther. 11 (2020) 517.
[33] S. Banerjee, H. Cui, N. Xie, Z. Tan, S. Yang, M. Icyuz, V.J. Thannickal, E. Abraham, G. Liu, miR-125a-5p regulates differential activation of macrophages and inflammation, J. Biol. Chem. 288 (2013) 35428–35436.
[34] G.S. Li, L. Cui, G.D. Wang, miR-155-5p regulates macrophage M1 polarization and apoptosis in the synovial fluid of patients with knee osteoarthritis, Exp. Ther. Med. 21 (2021) 68.
[35] Y. Liu, X. Zhang, C. Gao, H. Zhang, H. Zhang, J. Qu, MicroRNA124 and microRNA21-5p regulate migration, proliferation and differentiation of rat bone marrow mesenchymal stem cells, Biosci. Rep. (2020) 40.
[36] W. Ren, J. Hou, C. Yang, H. Wang, S. Wu, Y. Wu, X. Zhao, C. Lu, Extracellular vesicles secreted by hypoxia pre-challenged mesenchymal stem cells promote non-small cell lung cancer cell growth and mobility as well as macrophage M2 polarization via miR-21-5p delivery, J. Exp. Clin. Cancer Res. 38 (2019) 62.
[37] P. Zhang, H. Wang, X. Luo, H. Liu, B. Lu, T. Li, S. Yang, Q. Gu, B. Li, F. Wang, X. Sun, MicroRNA-155 inhibits polarization of macrophages to M2-type and suppresses choroidal neovascularization, Inflammation 41 (2018) 143–153.
[38] B. Su, H. Han, Y. Gong, X. Li, C. Ji, J. Yao, J. Yang, W. Hu, W. Zhao, J. Li, G. Zhang, L. Zhou, Let-7d inhibits intratumoral macrophage M2 polarization and subsequent tumor angiogenesis by targeting IL-13 and IL-10, Cancer Immunol. Immunother. 70 (2021) 1619–1634.
[39] Y. Wu, H. Li, J. Xie, F. Wang, D. Cao, Y. Lou, miR1395p affects cell proliferation, migration and adipogenesis by targeting insulinlike growth factor 1 receptor in hemangioma stem cells, Int. J. Mol. Med. 45 (2020) 569–577.